# Performance of tungsten fibers for $W_f$/W composites under cyclic tensile load

**D. Terentyev[1], A. Dubinko[1], J. Riesch[2], S.Lebediev[3], I. Volkov[3], E.E. Zhurkin[4]**

[1]*Structural Materials Group, Institute of Nuclear Materials Science, SCK·CEN, Mol, 2400, Belgium*

[2]*Max-Planck-Institut für Plasmaphysik, 85748 Garching, Germany*

[3]*V.N. Karazin Kharkiv National University, 4 Svobody Sq., Kharkiv, 61022, Ukraine*

[4]*Peter the Great St. Petersburg Polytechnic University (SPbPU), Russia, 195251, St. Petersburg, Polytechnicheskaya, 29*

Abstract

Toughness improved tungsten-based composites are one of the currently considered material option for future fusion reactors capable to withstand both high heat flux and irradiation induced embrittlement. Today, fiber-reinforced composites ($W_f$/W) are being intensively studied as risk-mitigation materials to replace bulk tungsten which is susceptible to neutron irradiation embrittlement especially below 800°C. Operation of a material as an element of a plasma facing component (i.e. divertor monoblock or first wall armour) implies not only high heat flux exposure but also thermal cyclic fatigue caused by repetitive oscillations of the heat loads due to the nature of the plasma and the limitations on the capacity of its confinement. In this work, we assessed the performance of potassium doped tungsten fibers under cyclic loading applied in tensile mode. Stress-controlled fatigue tests were performed at room temperature, 300°C and 500°C increasing the load from 50% of the yield strength up to the ultimate tensile strength of the studied fibers. It is revealed that significant cyclic hardening emerges as the fatigue stress limit exceeds the yield strength already within a few cycles. Despite the noticed cyclic hardening, the wire can sustain few hundreds of cycles without any detectable damage unless the cycle stress is increased to reach the value above the mean ultimate tensile strength. Given this observation, we have studied the impact of the cyclic stress ($\sigma_C$) on the rupture strength and total elongation of the wires exposed to twenty loading cycles varying test temperature in the range 23-500°C. At room temperature, the rupture stress after cyclic deformation progressively increases with $\sigma_C$ and saturates at 2.7 GPa with a moderate reduction of the total elongation, while the nominal ultimate tensile strength of the wire is 2.5 GPa. Thus, the strength of the wire is increased by 200 MPa, on average. At elevated temperature, the rupture stress after the cyclic deformation increases by more than 300 MPa.

Keywords: Tungsten, fiber, cyclic fatigue, potassium doped, composites.

corresponding author: dterenty@sckcen.be

## 1. Introduction

Extension of the operational temperature/power range while sustaining required toughness and strength is a typical challenge in the design new materials and composites for nuclear applications [1]. Tungsten is a promising plasma facing material for nuclear fusion applications as it offers unique properties while being commercially achievable and sufficiently abundant [2]. However, due to

intrinsically high brittle to ductile transition temperature [3-5], the fracture toughness of tungsten needs to be improved envisaging the impact of neutron irradiation to which the plasma facing components (PFC) are exposed during the nuclear operation phase where the fusion energy is released as 3.5 helium and 14 MeV neutron. The embrittlement induced by the 14 MeV neutrons [6, 7], which severely impacts the fracture toughness of bulk tungsten metal is one of the most critical issues still to be addressed by material science and engineering communities .

To increase the toughness in general and mitigate the potential risk of the irradiation embrittlement, tungsten fiber-reinforced composites, consisting of W fibers (made of W wire) coated by an engineered interface and embedded in a W matrix, have been studied over the last decade in the frame of the European fusion program (se e.g. [8, 9]). In these composites, the interaction of fiber and matrix introduces extrinsic mechanisms of energy dissipation mitigating stress peaks and thus increasing the resistance against failure i.a. toughness. Hence, the development of $W_f$/W composite is considered as one of the options to mitigate the operational embrittlement [8]. The properties of W wire , being used as reinforcing fibers, are therefore critical with respect to the performance and operational fatigue of the composites. In that respect, the properties of tungsten fibers ($W_f$) has been intensively explored in the last decade [8, 10, 11].

In fact, the drawn tungsten wire was already commercially applied more than 100 years ago in the illumination industry as the main filament element for street lighting [12]. The problem of creep and thermal fatigue (light on - light off) lead to the discovery of potassium (K) doping [13, 14]. It was recognized that K-doping suppresses recrystallization and grain growth by forming precipitates at grain boundaries, thereby preventing their thermal diffusion and coarsening [15]. More recent research was therefore focused on the understanding of the extension of the positive impact of K-doping with respect to the thermal stability of the microstructure at very high temperatures (required for the sintering of the composites or expected in the fusion environment due to plasma instabilities), as well as the evolution of mechanical properties of the annealed wires.

The tensile mechanical properties and evolution of the microstructure under progressive annealing of pure W and K-doped wires were studied at room and elevated temperatures by groups of Riesch [16-19] and Terentyev [20-23]. The primary conclusion that can be drawn from those studies is, that the potassium doping helps suppressing massive grain growth at least up to 1600°C for 30 min, leading to a ductile behavior at room temperature with ultimate tensile strength exceeding 1 GPa. Annealing above 1900°C causes strong reduction of the tensile strength at elevated temperature (down to ~0.1 GPa at 500°C) and makes the wire fully brittle at room temperature. The tensile properties of the as-drawn wires, obtained in Ref.[20], are characterized by the monotonic reduction of UTS from ~2.5 GPa down to 1.6 GPa, while the test temperature raises from RT up to 600°C. In the same interval of test temperature, the elongation to fracture reduces from ~2.5% to 1%. The fracture mode is ductile necking, originated from the elongation and debonding of sub-grains, which causes the formation of so-called knife-edge pattern. A macroscopic neck is formed and the actual reduction in area (i.e. reduction of the wire diameter at the fracture position) increases with raising the test temperature.

There is already quite detailed information on wire's strength obtained from the uniaxial tensile loading, while the impact of cyclic loading still needs to be understood. Indeed, in addition to the embrittlement induced by 14 MeV neutrons [6, 7], the cyclic heat loads will contribute not only to the recrystallization and grain growth [2] but will eventually cause thermo-mechanical fatigue and cracking. For instance, in the case of ITER, regular plasma instabilities called "edge-localised modes" (ELM) are expected with estimated thermal power density around 1-10 GW $m^{-2}$ deposited onto the divertor surface in ~0.2-0.5 ms duration occurring with a frequency of ~1 Hz [24]. In addition to the regular plasma instabilities, the increase of the power load from 10 MW/$m^2$ up to 20 MW/$m^2$ is

envisaged during the slow transient events expected to occur within 10 sec (see e.g. [25]and the recent review by Hirai et.al. [26]). In the case of slow transients, depending on the position in the divertor monoblock, thermal stresses may exceed the yield strength limit causing irreversible plastic deformation.

In the past, limited number of studies have address the fatigue life of tungsten [27-32]. Both stress- and strain-controlled tests were performed on bulk tungsten in the as-forged and recrystallized state as well as information on the single crystal is available. The overall conclusion done from those works was that for the as-rolled tungsten the obtained data is in good agreement with the "universal slope" equation [33], while for the recrystallized material the obtained results fall considerably below the prediction (i.e. the prediction overestimated the fatigue endurance), especially for low cycle fatigue data range [27]. This finding pointed out some limitations of the application of the "universal slope" method to predict the fatigue endurance. Habainy et.al [31] have studied the fatigue endurance under tensile stress-controlled loading conditions using commercially pure tungsten supplied by AT&M (China) in forged and rolled states. The fatigue limit at room temperature was found to be 150-175 MPa (depending on mechanical treatment), and it was in the range of 250-300 MPa for the tests done at 280°C and 480°C. It was noticed that the surface treatment of the gauge section plays a role in the fatigue endurance.

Up to now, no information about the influence of cyclic fatigue on the tensile properties of tungsten wire is available in literature. Therefore, as a firsts step, we have investigated the tensile properties of K-doped wires exposed to cyclic fatigue in pure tensile loading mode. Due to the extremely small diameter of the wire, conventional strain-control measurements cannot be applied. Thus, stress-controlled tests were performed at elevated and room temperature. The fatigue stress was varied in a wide range starting from 50% of the yields stress and reaching the ultimate tensile strength (UTS) of the wire. The pre-fatigued wires, if not ruptured during the fatigue load, were then tensile tested up to fracture using the same strain rate as in fatigue loading. The microstructure of the fractured wires was investigated by scanning electron microscopy to reveal whether the deformation mechanism changed due to the fatigue pre-load.

## 2. Materials and experimental procedures

### 2.1 Tungsten wires

Drawn potassium doped (60–75 ppm) tungsten wires, identical to the wires used in [20, 21, 34] were provided by the OSRAM GmbH, Schwabmünchen. The diameter of the wires was measured to be 148.7 ± 0.2 µm [34]. Measurements were performed by high resolution optical microscopy. Basic information of the grain microstructure of the wires in the as-received condition has been reported in [18, 20, 21, 34]. The grains are essentially elongated (i.e. large width-to-wide aspect ratio, typically exceeding 10) in the direction of wire axis and form curled structure in the wire cross-section. The size of grains in the wire's cross-section varies from 0.1 up to 1 µm. In the longitudinal cross-section, the interior of grains was reported to contain high density of dislocation defects and dislocation boundaries [18]. The grain size along the wire axis was estimated to be in the range 10-40 µm.

### 2.2 Test procedure and methodology to assess the impact of cyclic load

The fatigue pre-load was performed on the same test bench with electro-actuator as used in our previous works, dedicated to the assessment of the tensile properties of W wires [21, 22]. However, to ensure the rigidity of the displacement under multiple cycle loads at high temperature (up to 500°C),

new pull rods and sample holders were fabricated from Inconel 618 grade. The wires were cut into pieces of 100 mm (called fibers in the following) and these were used to prepare the samples for the cyclic loading tests. The straightened, as was applied in our earlier works [21, 22], and cut wire pieces were clamped between two flat polished plates also made of Inconel 618.

To ensure constant temperature during the test, the gauge section of the sample and inner parts of the holders were placed inside a cylindrical furnace. The ramp time to reach the maximum temperature and the hold time prior to start the loading was 1 hours each. An uniaxial mechanical load was applied by a pull rod driven by an electrical gear box, with a load cell of 0.2 kN. A constant displacement rate of 5 µm/s was applied for regular tensile tests and fatigue tensile loadings. The load, measured by a strain gauge, was registered with a frequency of 0.3 Hz. The relative error on the measurement of the pull rod displacement is ± 0.1 % and the absolute error on the stress measurement is 15 MPa. The actual gauge section was 30 mm and the sample holder was equipped with a guide rail to ensure perfect alignment before and during the test. More details about testing procedure can be found in our earlier work [20, 22].

At first, the wire was tensile tested at room temperature (RT), 300°C and 500°C to obtain the reference stress-strain curves, given that new pull rods were applied. At least five valid tests were performed for each temperature to obtain the reference stress-strain relationship, the proof stress (corresponding to the yield strength) and the mean UTS as well as its distribution. Typical stress-strain curves are shown in Fig.1(a). As a result of the reference tests, the yield strength/proof stress $\sigma_{0.2\%}$ (σ at 0.2% of the strain as measured by the displacement of the pull road) of the wire at RT was determined to be about 1.9±0.1 GPa. The ultimate tensile strength (UTS) was determined to be 2550 ± 65 MPa, 2210 ± 85 MPa and 2090 ± 120 MPa at, respectively, RT, 300 °C and 500 °C. These values deviates about 5% to our previous results using the old pull rods (made of brass) . With the old set of pull rods, the UTS was measured to be 2423±40 MPa at RT temperature which makes a difference of 5% and similar difference is applied to the results at elevated temperature.

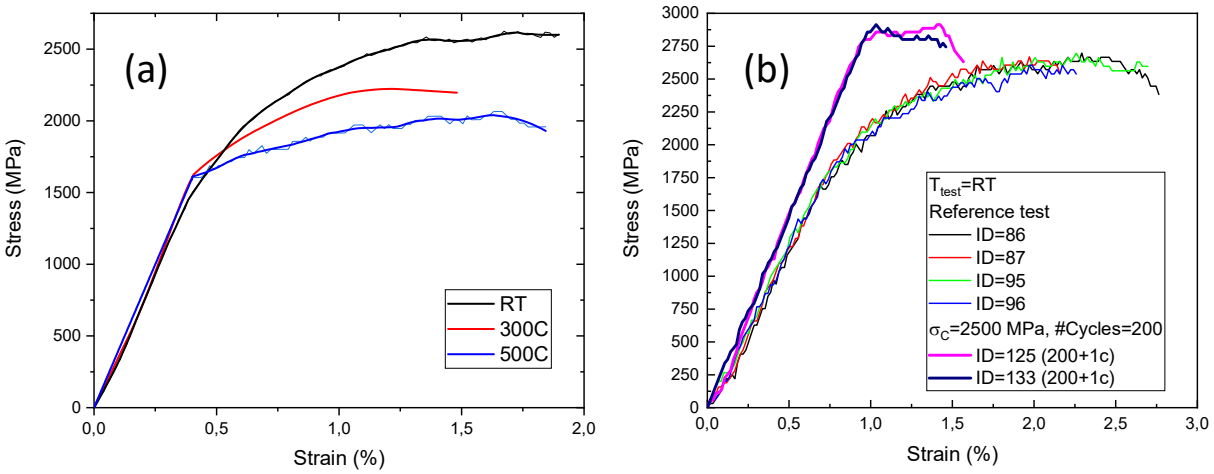


Fig.1. (a) Typical stress-strain curves obtained for the K-doped wire tested in tensile uniaxial load with loading rate of 5 µm/s at room temperature (RT), 300 °C and 500 °C. (b) Comparison of reference

stress-strain curves (for four randomly selected samples) and stress-strain curve obtained for the wires exposed to 200 loading cycles with the cycle stress of 2500 MPa.

We have performed the cyclic load tests in the stress-controlled mode and only in tension. We choose this load regime because the attachment of the clip gauge is practically impossible given the dimension of the wire, while the compressive load cannot be applied to the wire, as it will bend. The initial idea of the study was to determine the endurance of the wire against cyclic load in the low cycle fatigue mode i.e. by applying a relatively high cyclic stress. The maximum number of cycles to investigate was set as 200 since this is close to the number of high heat load pulses of 20 $MW/m^2$ required to qualify the plasma facing components with respect to the impact of the slow transient events.

In order to define a testing procedure we conducted a series of pre-tests based on the determined proof stress and UTS. The first series of tests were performed by taking the cycle stress ($\sigma_C$) below the proof stress and close to the lower bound of the mean UTS, namely 1.5 and 2.5 GPa. At least five tests with 200 cycles each were performed for each above mentioned cyclic stress and none of the tested wires ruptured during the loading. We have performed scanning electron microscopy (SEM) characterization on several wires in order to investigate possible presence localized deformation (signs of necking or plastic deformation at the surface) but none were found. To understand how the mechanical properties of the wire were changed after the cyclic load, we have performed tensile test until fracture after the $200^{th}$ cycle. We found that for all the wires the UTS was exceeding 2.5 GPa with a mean value of 2.65 GPa ($\sigma_C$=1500 MPa) and 2.75 GPa ($\sigma_C$=2500 MPa), respectively, for the lower and higher cyclic stress. An example of stress-strain curves for a wire fatigued at $\sigma_C$=2500 MPa is shown in Fig.1(b) together with several reference stress-strain curves (no fatigue load applied). As one can see, the fatigued wires start to yield at a stress exceeding 2700 MPa and exhibit limited ductility of less than 1%. This result means that fatigue-induced strengthening is significant enough to make the UTS of the wire higher than in the as-received state. Moreover, by checking the load-displacement curves it becomes evident that the cyclic hardening is established within several first loading cycles and the load-displacement response remains unchanged during the remaining cycles. This is shown in Fig.2, where the load-time diagram is shown for the $1^{st}$, $2^{nd}$, $3^{rd}$, $10^{th}$ , $100^{th}$ and $200^{th}$ cycle.

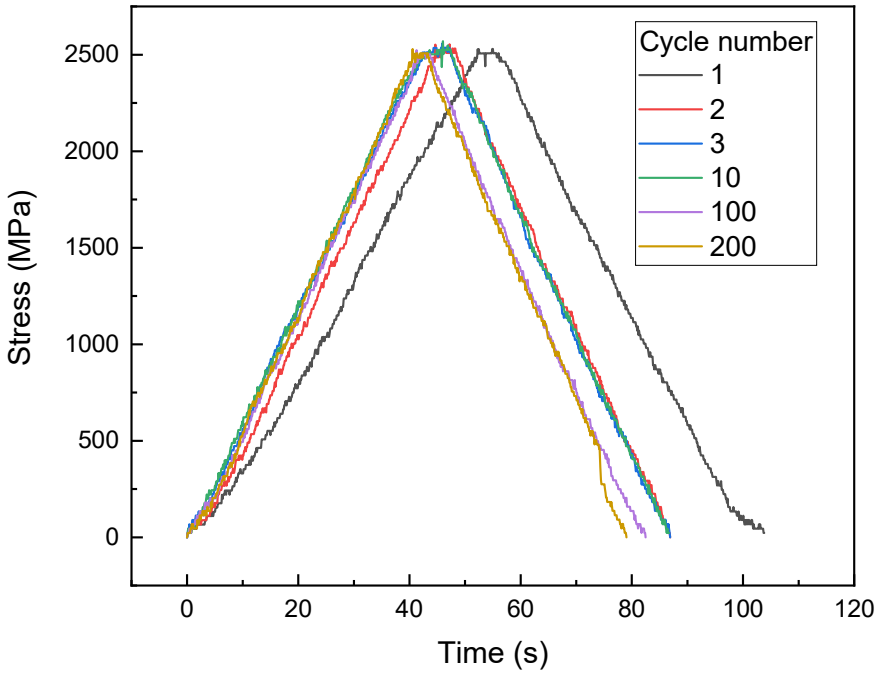


Fig.2. Stress-time diagram for the first three, the tenth, the hundredth and the last loading cycles performed at room temperature at $\sigma_C$=2500 MPa. The displacement is expressed as time, the loading rate is 5 µm/s.

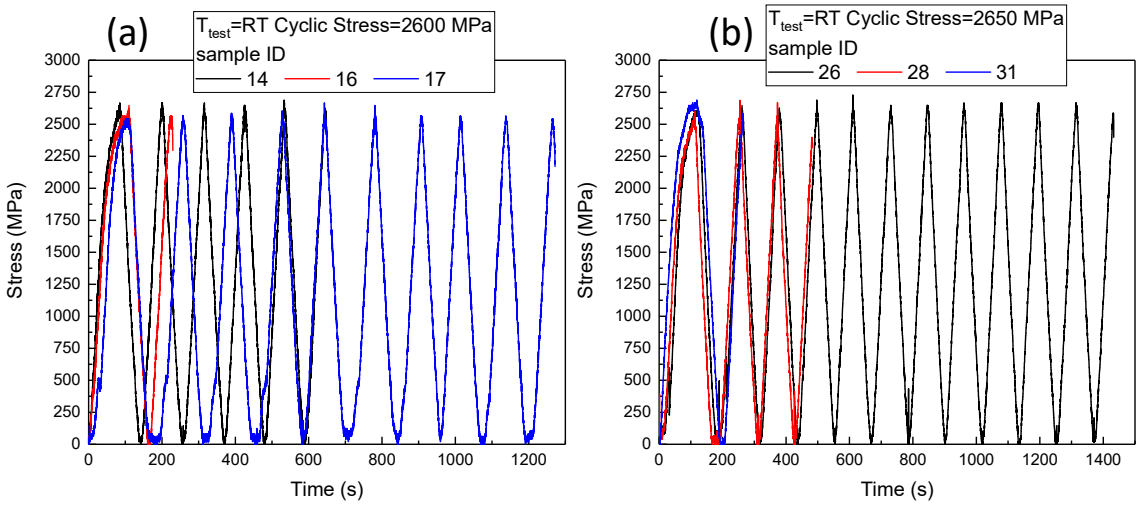


Fig.3. Stress-time curves obtained for the wires exposed to cyclic load at room temperature in the stress-controlled regime at (a) $\sigma_C$=2600 MPa and (b) $\sigma_C$=2650 MPa.

The next set of tests was performed also at room temperature with the cyclic stress in the range of the mean UTS on its upper side. In this case, we found that a rupture of the samples frequently occurs. The example of several load histories is shown in Fig.3 (a) and (b) for, respectively, $\sigma_C$=2600 MPa and (b) $\sigma_C$=2650 MPa. The fracture of the wires, if occurred, usually happened within less than 10 cycles.

The fracture usually occurred at the loading phase, but some wires (e.g. see Fig.(a) sample ID =16) ruptured at the unloading phase as well. In most of the cases the wire fracture took place at or just near by the maximum load. Following the statistics on rupture during the cyclic loading, we could see that if the wire sustains first few cycles (i.e. about 5) the rupture rarely occurs within next 15 cycles.

The surface microstructure of the wires ruptured in one cycle and during the fatigue load was studied by SEM, however, no specific difference in the features of fracture surface were found. In both cases (i.e. fatigue-rupture and single tensile test) the fracture surface consists of the delaminated sub-grains (so-called knife-edge structure) and multiple radial cracks. Fig.4 shows a comparison of the fracture surface of the wires ruptured in a single tensile test and after 2, 10 and 12 fatigue cycles at $\sigma_C$=2600 MPa.

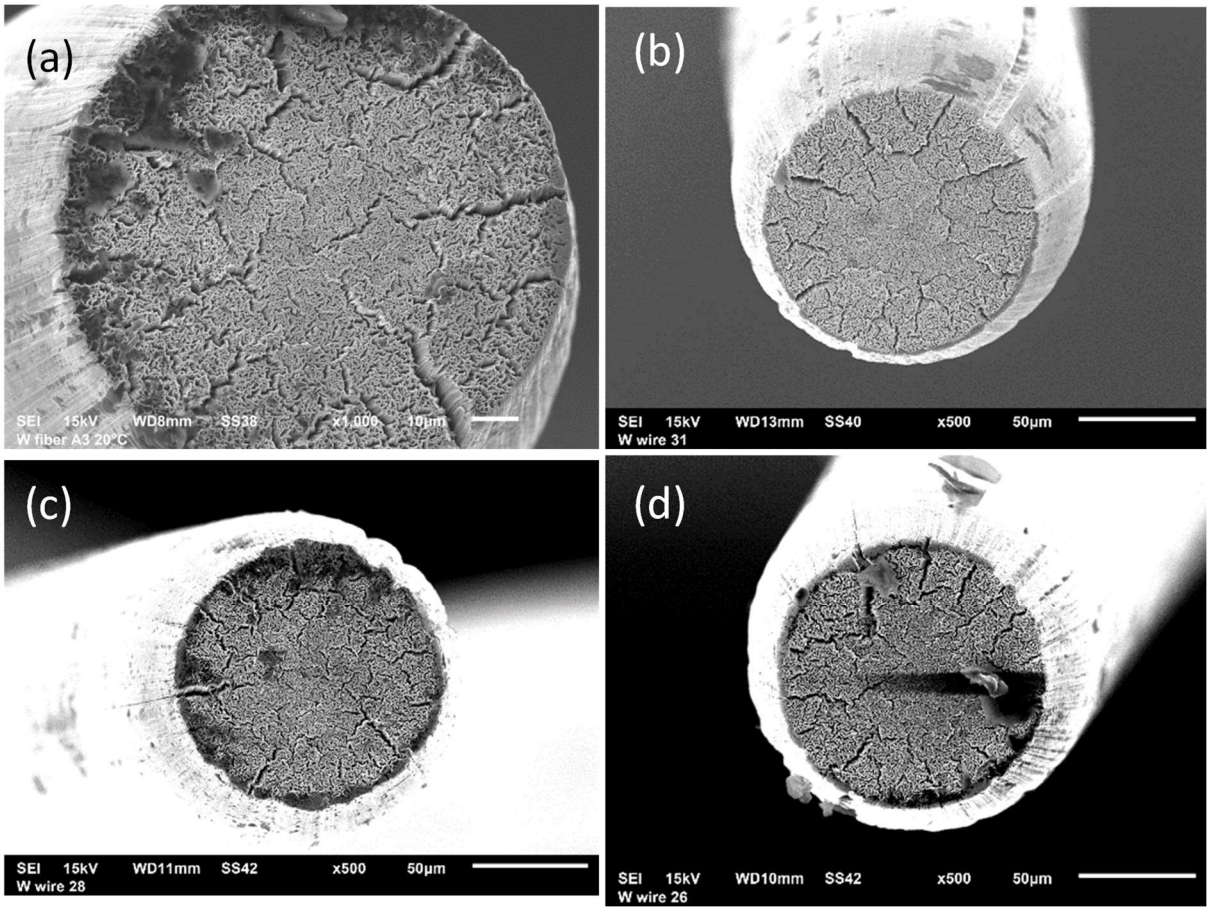


Fig.4. SEM micrographs of the wire fractured at room temperature. (a) reference microstructure obtained in the tensile test, UTS=2520 MPa; (b) fractured after two cycles at $\sigma_C$=2600 MPa; (c) fractured after 10 cycles at $\sigma_C$=2600 MPa; (d) fractured after 12 cycles at $\sigma_C$=2600 MPa.

Similar assessment was performed for the cyclic load at 300°C resulting in the same conclusion i.e. as long as $\sigma_C$ does not exceed the lower bound of the mean UTS (obtained using reference tensile tests at the same temperature), the wire sustains 200 cycles without any obvious change. The tensile test performed after the 200$^{th}$ cycle showed that the wire ruptured at the stress considerably exceeding the mean UTS of the reference wire. Thus, the fatigue-induced hardening at 300°C also leads to the strengthening of the wire and again, following details of the load-displacement cycles, the strengthening effect saturates within a few first cycles. Increasing the cyclic stress above the mean UTS

by 50-100 MPa (by 2%-4% of UTS) leads to the strong reduction of the fatigue endurance resulting in the wire rupture usually within less than 10 cycles.

Because of these observations valid at both RT an 300°C, instead of performing high number of cycles, we decided to investigate the relationship between the cyclic load stress, cyclic test temperature and resulting strength of the pre-fatigued wire. We do this by tensile testing (until fracture) of pre fatigued samples. Given that the fatigue-induced strengthening is established within several cycles (usually less than 5 loading cycles, and on-cycle rupture is observed usually at less than 10 cycles), we take 20 fatigue cycles to be a representative number to investigate the cyclic strengthening induced in the wire. In the following section, the results are presented in terms of stress-strain diagrams obtained for the pre-fatigued wires at RT, 300 °C and 500 °C. The mean UTS, total elongation and fracture surface are reported and compared with the reference measurements.

## 3. Results

### 3.1 Impact of cyclic load at RT

In the case of tests done at RT, we have studied a large interval of the applied cyclic stress from 500 MPa up to 2650 MPa. For each applied cyclic stress at least five valid tests were performed. At 2650 MPa, approximately a half of the samples survived 20 cycles. Starting from $\sigma_C$=2700 MPa none of the samples survived 20 cycles. The resulting stress-strain curves for loads where the fibers survived all 20 cycles are presented in Fig.5. As one can see the increase of the cyclic stress leads to a progressive increase of the rupture strength of the pre-fatigued wire. The effect on the total elongation is not so clear. For some tests there is a reduction (see Fig. 5 a) whereas for some tests it increases (see Fig.5 c). There is a trend for the reduction of the elongation if the cyclic stress approaches or exceeds the mean UTS. Thus, above a certain cyclic stress, the higher the rupture strength is the lower the total elongation.

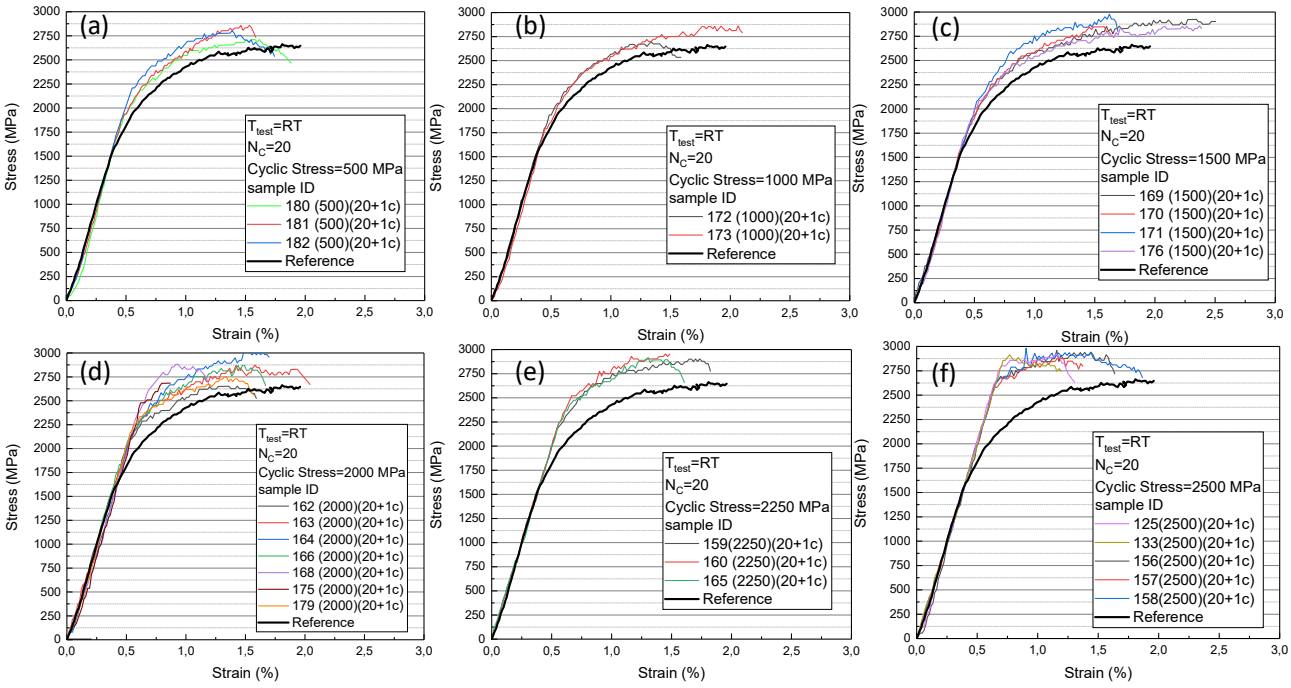

Fig.5. Example of stress-strain curves obtained for the pre-fatigued samples at RT for (a) $\sigma_C$=500 MPa; (b) $\sigma_C$=1000 MPa; (c) $\sigma_C$=1500 MPa; (d) $\sigma_C$=2000 MPa; (e) $\sigma_C$=2250 MPa; (f) $\sigma_C$=2500 MPa. Notion "20+1" on the legends means that the sample was tested till rupture after 20 fatigue cycles.

The average rupture strength and its standard deviation versus the cyclic stress is plotted in Fig.6. Given the provided standard deviation, we can state that the rupture strength of the pre-fatigued wire increases with the raise of the cyclic stress and saturates around the value of 2.7 GPa. The saturation occurs at $\sigma_C$=1000 MPa. As soon as $\sigma_C$ exceeds 2600 MPa, the rupture stress starts to decrease. At $\sigma_C$=2650 MPa, the average rupture strength is 2630 MPa which means that some of the wires did not sustain 20 cycles. There is a drop in the rupture strength at 2000 MPa but to make a firm conclusion on whether this is a real effect or it is caused by a relatively large spread in the values further extensive test programme is required. The average total elongation is presented in Fig.7, which shows that the elongation remains constant up to $\sigma_C$=1500 MPa and decreases down to 0.8% at $\sigma_C$=2500 MPa and then again stays constant for a larger cyclic stress. Note that even in the reference state, there is a significant spread of the total elongation of the wire, which originates from the surface roughness (due to extrusion process) which likely acts as source of stress-localization causing necking and subsequent rupture.

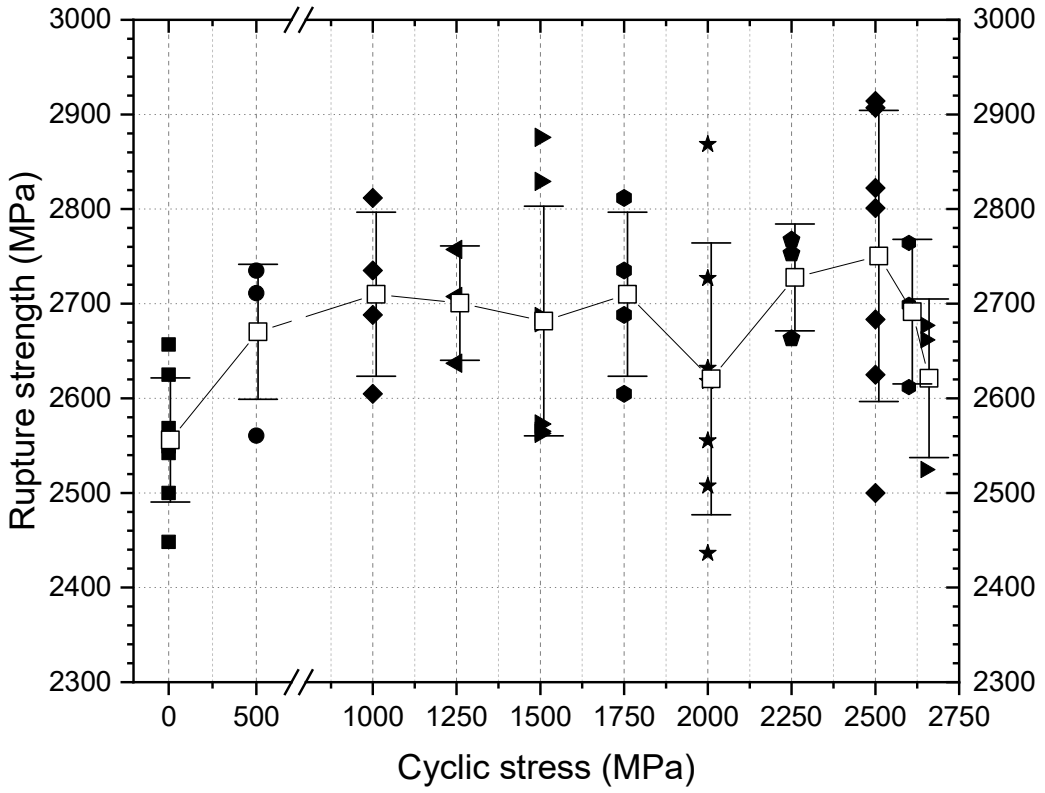


Fig.6. The average rapture strength and its standard deviation versus the cyclic stress measured at RT. The absolute values for all successful tests are also added.

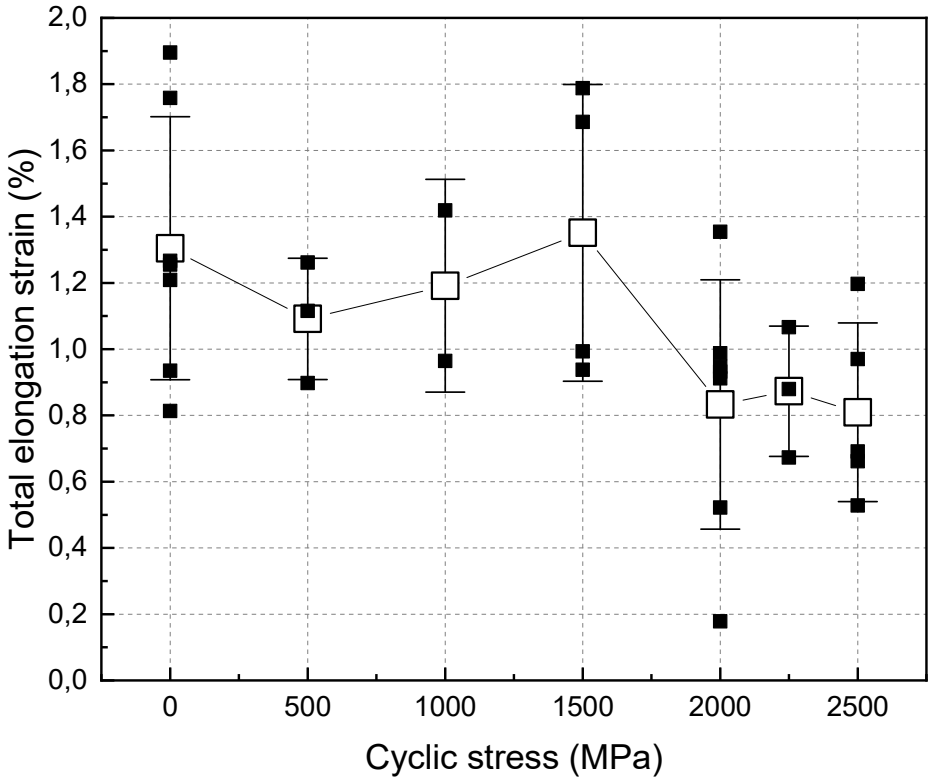


Fig.7. The average total elongation and its standard deviation versus the cyclic stress. The results are obtained at RT.

### 3.2 Impact of cyclic load at elevated temperature

At elevated temperature, we have performed the fatigue load (20 cycles) at three levels of the cyclic stress selected as 80%, 90% and 100% of the lower bound of the UTS measured in the standard tensile test at the corresponding temperature, see Section 2.2. Thus, at 300°C, the tests were performed at the cyclic stress of 1800, 2000 and 2200 MPa. At 500°C, the tests were performed at the cyclic stress of 1750, 1850 and 1950 MPa. An example of typical stress-strain curves is presented in Fig.8. As in the case of the results obtained at RT, an increasing the cyclic stress causes the increase of the rupture stress at both 300°C and 500°C. However, it is interesting to note that there is no evident decrease of the elongation (on average) unlike observed at RT tests when $\sigma_C$ reaches he mean UTS (see Fig.7). Secondly, we can see that the rupture strength of the pre-fatigued wires increases up to 2700 MPa and 2600 MPa, respectively, at 300°C and 500°C. Thus, the tensile fatigue damage at elevated temperature yields to much higher relative increase (compared to reference UTS) of the rupture strength compared to the result obtained at room temperature. This is very interesting and important result given that the UTS obtained in the standard tensile test shows that the wire strength monotonically decreases with test temperature. To understand better the physical reasons for the fatigue-induced strengthening in these wires one needs to perform transmission electron microscopy (TEM) and electron back scattering diffraction analysis (EBSD) to clarify potential increase of the dislocation density and grain refinement, which would explain the observed result. However, as discussed in our recent works [22, 35-37], especially TEM study is challenging due to the sample preparation requiring usage of focus ion beam (FIB) and subsequent flash polishing procedure, which

is not so well established for tungsten [38]. Assessment of deformation-induced dislocation density by EBSD is also challenging due to rather small initial grain size, which undergoes even further refinement after deformation.

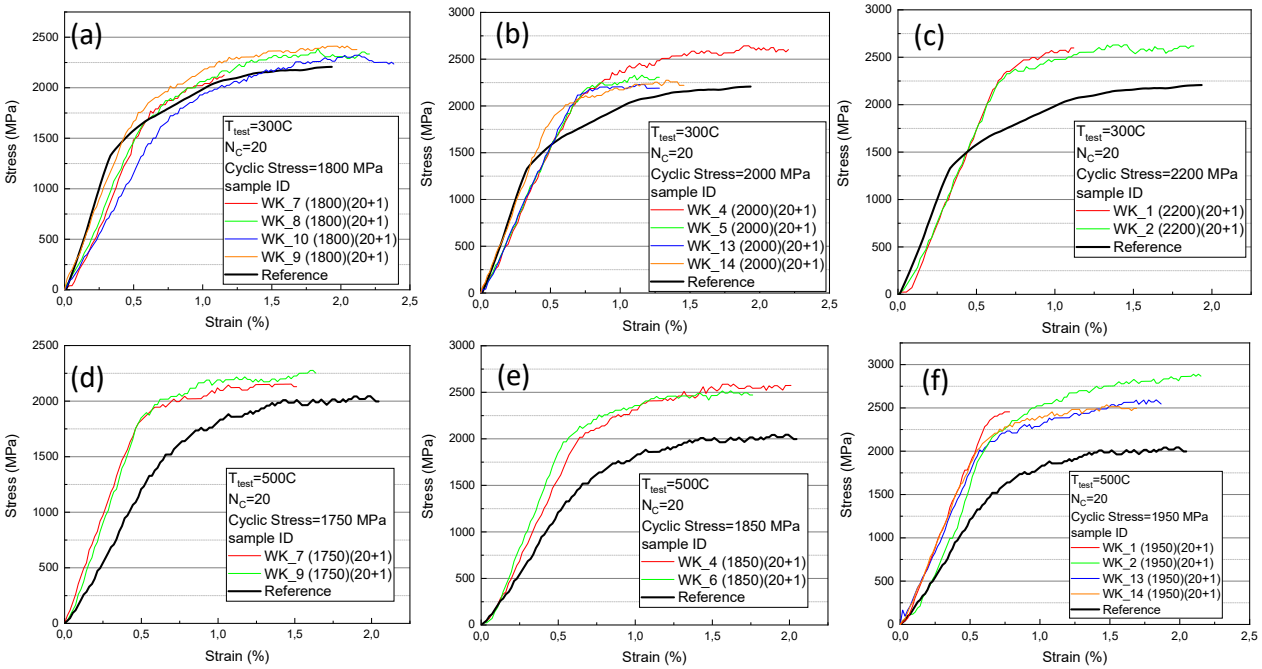


Fig.8. Example of stress-strain curves obtained for the pre-fatigued samples at 300°C for (a) $\sigma_C$=1800 MPa; (b) $\sigma_C$=2000 MPa; (c) $\sigma_C$=2200 MPa; and at 500°C (d) $\sigma_C$=1750 MPa; (e) $\sigma_C$=1850 MPa; (f) $\sigma_C$=1950 MPa. Note that for the same rupture stress the elongation could be very similar or quite different, see examples on (c) and (e).

SEM inspection was performed on at least three randomly selected wires per test condition. On some of the wires we found extended cracks, apparently formed via interconnection of radial cracks, going across the whole fractured surface. These extended cracks remarkably differ from typical radial micro-cracks. Examples of these cracks observed in 300°C and 500°C tests are shown in Fig.9. For instance in Fig.9 (a) and (b), one can see a dominant macro-crack, which could have developed as a result of bridging of smaller radial cracks during the cycle loading. Fig.9 (c) and (d) show the case of multiple differentiated macro-cracks. At this, on Fig.9(c) we see two parallel cracks developed from surface-to-surface, while in Fig.9(d) we see several radial macro-cracks. However, such macro-cracks were not observed on each pre-fatigued sample, and the fracture surface of many fatigued samples in fact looked very similar to the fracture surface of the reference samples deformed in single load run.

Nevertheless, let us discuss the morphology of cracks presented in Fig.9, as it is very well known that it is linked to the crack nucleation and its growth mechanisms. In fact, most of the cracks observed in this work are of intergranular type, transgranular fracture for the as-drawn wires has not been reported as long as tests were performed at room temperature and above. On Fig.9, one can see the fracture surface of the wires consist of three features: (i) knife-edge necked grains (present over the whole surface) – which represents delamination of several interconnected low angle grain boundaries; (ii) multiple radial micro-cracks (originating from the surface of the wire and extending towards its center) – which is delamination of several interconnected high angle grain boundaries; and (iii) one or two macro-cracks (per wire cross-section) which apparently form by the interconnection large radial cracks.

Delamination of sub-grains (as a result of local grain necking) should cause stress relieve upon cyclic loading. While the formation of radial cracks, their extension towards the center of the wire and interconnection into a macro-cracks effectively reduces the cross-section of the wire and thereby should cause a higher local stress in the necking region under progressive stress-controlled fatigue load. However, from the currently available results it is hard to say whether the macro-cracks such as shown in Fig.9 are indeed formed during the fatigue pre-load or occur during the last cycle of non-interrupted deformation performed to achieve the rupture.

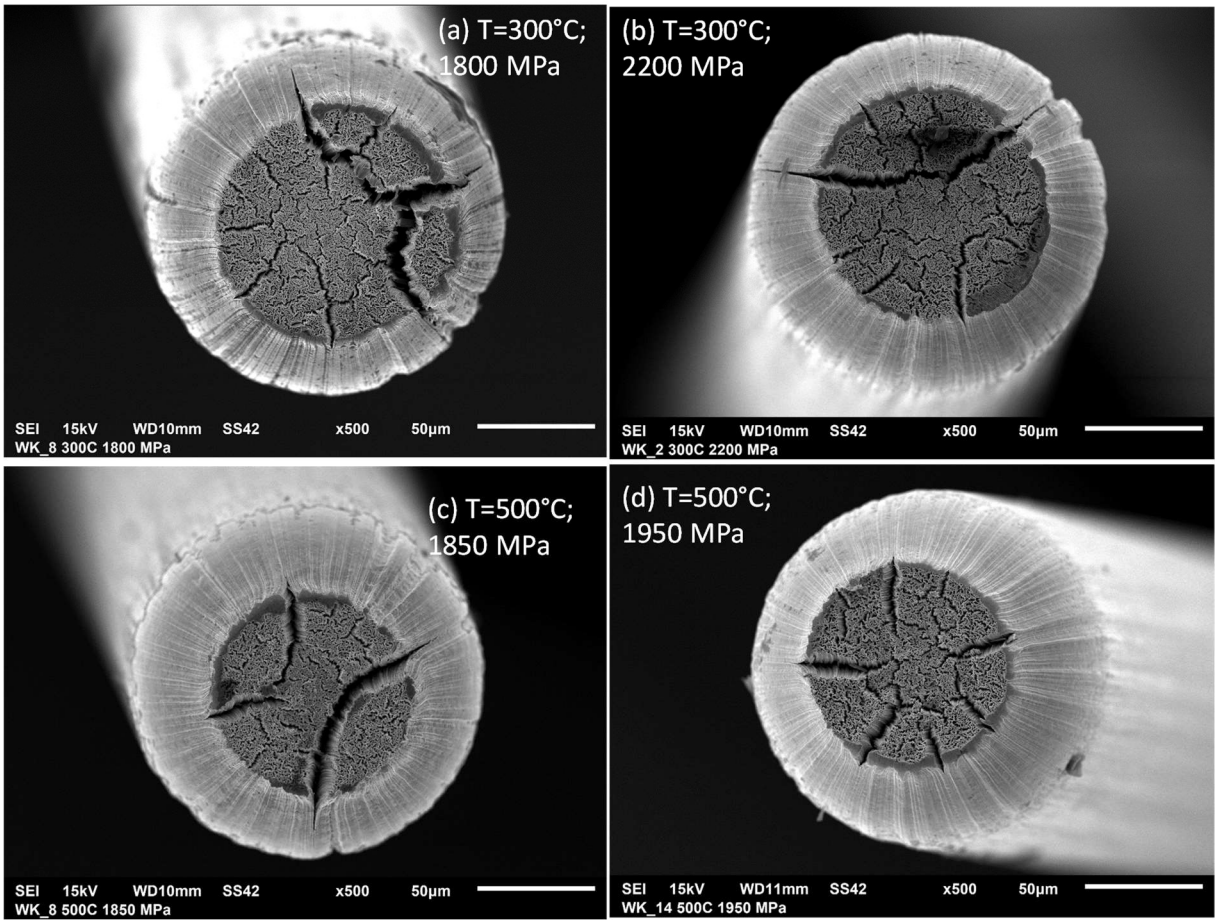


Fig.9. SEM micrographs showing the fracture surface of the tested pre-fatigued wires at (a) 300°C, $\sigma_C$=1800 MPa; (b) 300°C, $\sigma_C$=2200 MPa; (c) 500°C, $\sigma_C$=1850 MPa; (d) 500°C, $\sigma_C$=1950 MPa.

Finally, the impact of the cyclic stress and test temperature on the rupture stress of the wire is summarized in Fig.10. On this figure, the reference ultimate tensile strength of the wire corresponds to $\sigma_C$=0 MPa. As we can see, the tensile fatigue deformation at elevated temperature yields to much stronger increase of the rupture stress as soon as the applied cyclic stress exceeds 1800 MPa. Given that such raise in the rupture strength is observed at elevated temperature (300°C and above) and not at room temperature, one can suggest that pre-loading at the stress above 2000 MPa activates some strengthening mechanisms apparently driven by dislocation motion. Indeed, at RT screw dislocations still exhibit very low mobility [39-42], while at 300°C (and above) grain boundaries should limit plastic deformation in polycrystalline tungsten [43-46] (i.e. formation of dislocation pile-ups and tangles near

by the grain boundaries, as observed by TEM). Thus, one can suggest that at a level of 1.8 GPa of external tensile load, certain trans-grain irreversible (or partially reversible under unloading) plastic deformation is activated modifying the wire microstructure uniformly and making it much stronger compared to the reference microstructure. However, as mentioned above, the explanation of this results requires proper microstructure analysis, which is a significant volume of work to be done outside of the present study.

After the fatigue damage, the rupture strength of the wire becomes comparable to that retrieved at RT tests, being at the level of 2.6-2.7 GPa. Given this large capacity of the fatigue strengthening, it is not surprising why we did not observe any rupture of the wire tested within 200 cycles whenever the cyclic stress was kept below the lower bound of the UTS (measured at the same temperature).

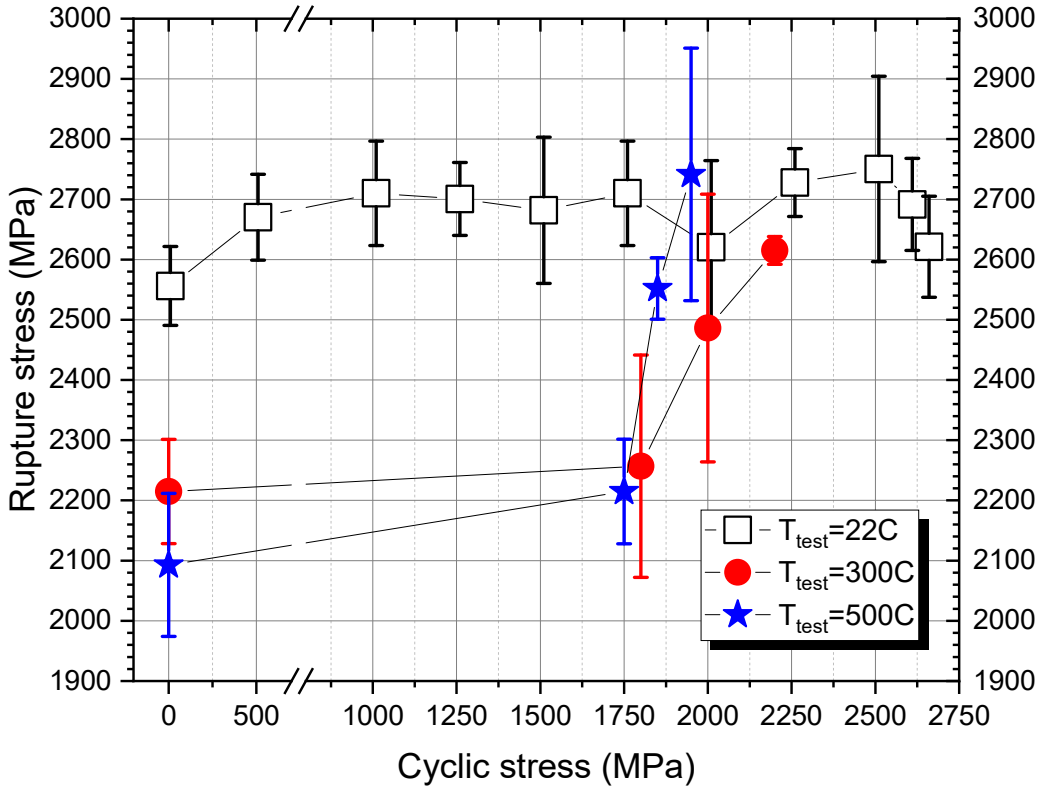


Fig.10. The average rapture strength and its standard deviation versus the cyclic stress obtained at RT, 300°C and 500°C.

**4. Summary and conclusions**

In this work, we have performed an experimental study of the impact of the tensile fatigue load on the rupture strength of K-doped tungsten wire with a diameter of 150 µm (same wire as studied in our previous works). The fatigue load was realized in the stress controlled regime. A particular focus was put on the understanding of the role of the fatigue cyclic stress and test temperature on the resulting wire strength and features of the fracture surface. The applied fatigue cyclic stress was varied in a wide

range starting from the value below the indicative yield stress and up to the upper boundary of the ultimate tensile strength range. The reference tensile tests had determined the mean ultimate tensile strength and its standard deviation to be 2550 ± 65 MPa, 2210 ± 85 MPa and 2090 ± 120 MPa at, respectively, RT, 300 °C and 500 °C.

On the basis of the obtained results, we can summarize the following statements:

(i) The stress-controlled fatigue tests performed at the cyclic stress corresponding to the lower bound of the ultimate tensile strength demonstrated that each tested sample (without evident surface defects) survived 200 cycles. This statement is valid for the tests performed at room temperature, 300°C and 500°C.

(ii) The stress-controlled fatigue tests performed at the cyclic stress exceeding the mean value of the UTS by ~2% (i.e. 1.02× mean UTS) demonstrated that none of the wires survived 20 cycles. This statement is valid for tests performed at room temperature.

(iii) For the wires pre-fatigued up to 20 cycles and tested at elevated temperature, it can be concluded that the tensile cyclic deformation yields to the well-resolved increase of the rupture strength. The increase of the rupture strength is also observed at RT but in smaller amount.

(iv) The microstructure of the pre-fatigued wires sometimes shows the presence of macro-cracks (grown from surface-to-surface or from surface to center) which are not so pronounced (speaking statistically) in the reference samples. However, far not every studied fatigued wire has such evident macro-cracks.

Quantitatively, the main outcome of this study appears to be a positive effect of the high stress fatigue pre-load on the strength of the wire when loaded up to the rupture, especially at elevated temperature. To confirm and rationalize the presently obtained result one needs to perform additional tests at elevated temperature increasing the fatigue cyclic stress as well as investigating the nano-scale changes in the microstructure induced by the tensile fatigue cyclic loads.

In the present study, the sample geometry and loading rate was chosen to correspond to the previous studies. For future studies, it might be important to investigate the impact of the gauge length and loading rate, which should be selected in compliance with the actual constraints within the composite material and the loading conditions expected during the heat loads critical for the assessment of crack propagation. In addition, our future work will include a parametric EBSD analysis to reveal the information on the grain and sub-grain structure in the deformed wires after the fatigue pre-load to understand whether it truly yields to changes in grain morphology or these are the sub-micrometer changes. An attempt to perform TEM analysis of the necked regions of the wire pre-fatigues wires is also planned.

**Acknowledgements**

This work has been carried out within the framework of the EUROfusion Consortium and has received funding from the Euratom research and training programme 2014–2018 under grant agreement No 633053. The views and opinions expressed herein do not necessarily reflect those of the European Commission. The work was partially supported by FOD grant of Belgium Government. The authors want to acknowledge support by Osram GmbH, Schwabmünchen, Germany for providing the tungsten wire and performing the annealing.

**References**

[1] S.J. Zinkle, J.T. Busby, Structural materials for fission & fusion energy, Materials Today 12(11) (2009) 12-19.
[2] G. Pintsuk, Tungsten as a Plasma-Facing material, (2012).
[3] A. Giannattasio, M. Tanaka, T.D. Joseph, S.G. Roberts, An empirical correlation between temperature and activation energy for brittle-to-ductile transitions in single-phase materials Physica Scripta T128 (2007) 87-90.
[4] A. Giannattasio, Z. Yao, E. Tarleton, S.G. Roberts, Brittle-ductile transitions in polycrystalline tungsten, Philosophical Magazine 90(30) (2010) 3947-3959.
[5] D.H. Lassila, F. Magness, D. Freeman, Ductile-Brittle Transition Temperature Testing of Tungsten Using the Three-Point Bend Test, Report Lawrence Livermore National Laboratory UCRL-ID-108258 (1991).
[6] A. Hasegawa, M. Fukuda, S. Nogami, K. Yabuuchi, Neutron irradiation effects on tungsten materials, Fusion Engineering and Design 89(7-8) (2014) 1568-1572.
[7] I.V. Gorynin, V.A. Ignatov, V.V. Rybin, S.A. Fabritsiev, V.A. Kazakov, V.P. Chakin, V.A. Tsykanov, V.R. Barabash, Y.G. Prokofyev, Effects of Neutron-Irradiation on Properties of Refractory-Metals, Journal of Nuclear Materials 191 (1992) 421-425.
[8] C. Linsmeier, M. Rieth, J. Aktaa, T. Chikada, A. Hoffmann, J. Hoffmann, A. Houben, H. Kurishita, X. Jin, M. Li, A. Litnovsky, S. Matsuo, A. von Muller, V. Nikolic, T. Palacios, R. Pippan, D. Qu, J. Reiser, J. Riesch, T. Shikama, R. Stieglitz, T. Weber, S. Wurster, J.H. You, Z. Zhou, Development of advanced high heat flux and plasma-facing materials, Nuclear Fusion 57(9) (2017).
[9] J.W. Coenen, S. Antusch, M. Aumann, W. Biel, J. Du, J. Engels, S. Heuer, A. Houben, T. Hoeschen, B. Jasper, F. Koch, J. Linke, A. Litnovsky, Y. Mao, R. Neu, G. Pintsuk, J. Riesch, M. Rasinski, J. Reiser, M. Rieth, A. Terra, B. Unterberg, T. Weber, T. Wegener, J.H. You, C. Linsmeier, Materials for DEMO and reactor applications-boundary conditions and new concepts, Physica Scripta T167 (2016).
[10] R. Neu, J. Riesch, A.V. Muller, M. Balden, J.W. Coenen, H. Gietl, T. Hoschen, M. Li, S. Wurster, J.H. You, Tungsten fibre-reinforced composites for advance d plasma facing components, Nuclear Materials and Energy 12 (2017) 1308-1313.
[11] S.J. Zinkle, J.T. Busby, Structural materials for fission & fusion energy, Materials today 12 (2009).
[12] P. Schade, 100 years of doped tungsten wire (vol 28, pg 647, 2010), Int J Refract Met H 29(4) (2011) 559-559.
[13] C.L. Briant, E.L. Hall, The Microstructure of Rolled and Annealed Tungsten Rod, Metall Trans A 20(9) (1989) 1669-1686.
[14] C.L. Briant, B.P. Bewlay, The Coolidge Process for Making Tungsten Ductile - the Foundation of Incandescent Lighting, Mrs Bull 20(8) (1995) 67-73.
[15] E. Pink, L. Bartha, The metallurgy of doped/non-sag tungsten, Elsevier Science Publishers (1989).
[16] J. Riesch, T. Hoschen, C. Linsmeier, S. Wurster, J.H. You, Enhanced toughness and stable crack propagation in a novel tungsten fibre-reinforced tungsten composite produced by chemical vapour infiltration, Physica Scripta T159 (2014).
[17] J. Riesch, M. Aumann, J.W. Coenen, H. Gietl, G. Holzner, T. Hoschen, P. Huber, M. Li, C. Linsmeier, R. Neu, Chemically deposited tungsten fibre-reinforced tungsten - The way to a mock-up for divertor applications, Nuclear Materials and Energy 9 (2016) 75-83.
[18] P. Zhao, J. Riesch, T. Hoschen, J. Almanstotter, M. Balden, J.W. Coenen, R. Himml, W. Pantleon, U. von Toussaint, R. Neu, Microstructure, mechanical behaviour and fracture of pure tungsten wire after different heat treatments, Int J Refract Met H 68 (2017) 29-40.
[19] J. Riesch, A. Feichtmayer, M. Fuhr, J. Almanstötter, J.W. Coenen, H. Gietl, T. Höschen, C. Linsmeier, R. Neu, Tensile behaviour of drawn tungsten wire used in tungsten fibre-reinforced tungsten composites, Physica Scripta 2017 (2017) 014032.
[20] D. Terentyev, J. Riesch, S. Lebedev, A. Bakaeva, J.W. Coenen, Mechanical properties of as-fabricated and 2300 °C annealed tungsten wire tested up to 600 °C, Int J Refract Met H 66 (2017) 127-134.

[21] D. Terentyev, J. Riesch, S. Lebediev, T. Khvan, A. Zinovev, M. Rasiński, A. Dubinko, J.W. Coenen, Plastic deformation of recrystallized tungsten-potassium wires: constitutive deformation law in the temperature range 22-600°C, Int J Refract Met H 66 (2018) 127-134.
[22] D. Terentyev, J. Riesch, S. Lebediev, T. Khvan, A. Zinovev, M. Rasiński, A. Dubinko, J.W. Coenen, Strength and deformation mechanism of tungsten wires exposed to high temperature annealing: impact of potassium doping, International Journal of Refractory Metals and Hard Materials 76 (2018) 226-233.
[23] D. Terentyev, J. Riesch, S. Lebediev, T. Khvan, A. Dubinko, J.W. Coenen, EBSD maps of annealing tungsten wire: effect of pottasium doping on the recrystallization, International Journal of Refractory Metals and Hard Materials (2018) submitted.
[24] M. Wirtz, J. Linke, T. Loewenhoff, G. Pintsuk, I. Uytdenhouwen, Thermal shock tests to qualify different tungsten grades as plasma facing material, Physica Scripta T167 (2016) 014015.
[25] R.A. Pitts, S. Carpentier, F. Escourbiac, T. Hirai, V. Komarov, S. Lisgo, A.S. Kukushkin, A. Loarte, M. Merola, A.S. Naik, R. Mitteau, M. Sugihara, B. Bazylev, P.C. Stangeby, A full tungsten divertor for ITER: Physics issues and design status, Journal of Nuclear Materials 438 (2013) S48-S56.
[26] T. Hirai, S. Panayotis, V. Barabash, Et.al., Use of tungsten material for the ITER divertor, Nuclear Materials and Energy 000 (2016) 1-7.
[27] R.E. Schmunk, G.E. Korth, Tensile and Low-Cycle Fatigue Measurements on Cross-Rolled Tungsten, Journal of Nuclear Materials 103(1-3) (1982) 943-947.
[28] R.E. Schmunk, G.E. Korth, M. Ulrickson, Tensile and Low-Cycle Fatigue Measurements on Cross-Rolled Tungsten at 1505-K, Journal of Nuclear Materials 122(1-3) (1984) 850-854.
[29] K.J. Bowman, R. Gibala, Cyclic Deformation of Tungsten Single-Crystals, Scripta Metall Mater 20(10) (1986) 1451-1454.
[30] R.C. Wetherhold, L.J. Westfall, Deformation of Surface Cladding and Matrix of Tungsten-Fiber-Reinforced Superalloy under Thermomechanical Loading, Mater Sci Eng 85(1-2) (1987) L13-L17.
[31] J. Habainy, S. Iyengar, Y. Lee, Y. Dai, Fatigue behavior of rolled and forged tungsten at 25 degrees, 280 degrees and 480 degrees C, Journal of Nuclear Materials 465 (2015) 438-447.
[32] W.H. Guan, S. Nogami, M. Fukuda, A. Hasegawa, Tensile and fatigue properties of potassium doped and rhenium containing tungsten rods for fusion reactor applications, Fusion Engineering and Design 109 (2016) 1538-1542.
[33] S.S. Manson, Exper. Mech. 5 (1965) 943-948.
[34] J. Riesch, Y. Han, J. Almanstotter, J.W. Coenen, T. Hoschen, B. Jasper, P. Zhao, C. Linsmeier, R. Neu, Development of tungsten fibre-reinforced tungsten composites towards their use in DEMO-potassium doped tungsten wire, Physica Scripta T167 (2016).
[35] D. Terentyev, W. Van Renterghem, L. Tanure, A. Dubinko, J. Riesch, S. Lebediev, T. Khvan, K. Verbeken, J.W. Coenen, E.E. Zhurkin, Correlation of microstructural and mechanical properties of K-doped tungsten fibers used as reinforcement of tungsten matrix for high temperature applications, Int J Refract Met H 79 (2019) 204-216.
[36] D. Terentyev, L. Tanure, A. Bakaeva, A. Dubinko, V. Nikolic, J. Riesch, K. Verbeken, S. Lebediev, E.E. Zhurkin, Micromechanical and microstructural properties of tungsten fibers in the as-produced and annealed state: Assessment of the potassium doping effect, Int J Refract Met H 81 (2019) 253-271.
[37] V. Nikolic, J. Riesch, M.J. Pfeifenberger, R. Pippan, The effect of heat treatments on pure and potassium doped drawn tungsten wires: Part II - Fracture properties, Mat Sci Eng a-Struct 737 (2018) 434-447.
[38] B. Horvath, R. Schaublin, Y. Dai, Flash electropolishing of TEM lamellas of irradiated tungsten, Nucl Instrum Meth B 449 (2019) 29-34.
[39] H.J. Lim, C.C. Battaile, J.D. Carroll, B.L. Boyce, C.R. Weinberger, A physically based model of temperature and strain rate dependent yield in BCC metals: Implementation into crystal plasticity, Journal of the Mechanics and Physics of Solids 74 (2015) 80-96.
[40] D. Brunner, V. Glebovsky, Analysis of flow-stress measurements of high-purity tungsten

single crystals, Materials Letters 44 (2000) 144-152.

[41] J. Stephens, Dislocation Structures in Single-Crystal Tungsten and Tungsten Alloys, Metall Trans 1 (1970) 1293.
[42] C.Y. Chiem, W.S. Lee, The Influence of Dynamic Shear Loading on Plastic-Deformation and Microstructure of Tungsten Single-Crystals, Mat Sci Eng a-Struct 187(1) (1994) 43-50.
[43] D. Terentyev, X.Z. Xiao, A. Dubinko, A. Bakaeva, H.L. Duan, Dislocation-mediated strain hardening in tungsten: Thermo-mechanical plasticity theory and experimental validation, Journal of the Mechanics and Physics of Solids 85 (2015) 1-15.
[44] X.Z. Xiao, D. Terentyev, A. Ruiz, A. Zinovev, A. Bakaev, E.E. Zhurkin, High temperature nano-indentation of tungsten: modelling and experimental validation, Materials Science & Engineering A accepted for publication (2019) in print.
[45] H. Sheng, G. Van Oost, E. Zhurkin, D. Terentyev, V.I. Dubinko, I. Uytdenhouwen, J. Vleugels, High temperature strain hardening behavior in double forged and potassium doped tungsten, Journal of Nuclear Materials 444(1-3) (2014) 214-219.
[46] A. Dubinko, D. Terentyev, A. Bakaeva, K. Verbeken, M. Wirtz, M. Hernandez-Mayoral, Evolution of plastic deformation in heavily deformed and recrystallized tungsten of ITER specification studied by TEM, Int. Journal of Refractory Metals and Hard Materials 66 (2017) 105-115.